KURENAI

Kyoto University Research Information Repository

KYOTO UNIVERSITY

Title	Cosmology from weak lensing of CMB
Author(s)	Namikawa, T.
Citation	Progress of Theoretical and Experimental Physics (2014), 2014(6)
Issue Date	2014-06-05
URL	http://hdl.handle.net/2433/189426
Right	© The Author(s) 2014. Published by Oxford University Press on behalf of the Physical Society of Japan.; This is an Open Access article distributed under the terms of the Creative Commons Attribution License (http://creativecommons.org/licenses/by/3.0/), which permits unrestricted reuse, distribution, and reproduction in any medium, provided the original work is properly cited.
Type	Journal Article
Textversion	publisher

Kyoto University

CMB Cosmology

Cosmology from weak lensing of CMB

Toshiya Namikawa[1],*

[1]*Yukawa Institute for Theoretical Physics, Kyoto University, Kyoto 606-8502, Japan*
*E-mail: namikawa@yukawa.kyoto-u.ac.jp

....
The weak lensing effect on the cosmic microwave background (CMB) induces distortions in
the spatial pattern of CMB anisotropies, and statistical properties of CMB anisotropies become
a weakly non-Gaussian field. We first summarize the weak lensing effect on the CMB (CMB
lensing) in the presence of scalar, vector, and tensor perturbations. Then we focus on the lensing
effect on CMB statistics and methods to estimate deflection angles and their power spectrum.
We end by summarizing recent observational progress and future prospects.
....
Subject Index E62, E63, E65

1. Introduction

The path of cosmic microwave background (CMB) photons emitted from the last scattering surface
of the CMB is deflected by the gravitational potential of the large-scale structure with typically a few
arcminutes deflection. This leads to distortion in the spatial pattern of observed CMB anisotropies.
Among various cosmological observations, a measurement of weak lensing signals in CMB maps is
a direct probe of intervening gravitational fields along a line of sight, and is considered as one of the
most powerful probes of fundamental issues in cosmology and physics in the near future.

Most of the pioneering work in CMB lensing focused on how the lensing effect modifies the two-
point statistics of CMB temperature anisotropies (e.g., [1–5] and references therein). An accurate
calculation of the lensing effect on the angular power spectrum in Ref. [5] showed that the acoustic
scale imprinted in the temperature is slightly smoothed and the small-scale temperature fluctuations
are enhanced by transferring large-scale power to the small scale. On the other hand, Refs. [6,7]
showed that the lensing effect also modifies the statistics of CMB anisotropies and generates non-
Gaussian signatures in the observed CMB anisotropies. A more interesting and important effect
for future studies of CMB lensing is that the gravitational lensing generates B-mode polarization
converted from E-mode polarization [8].

Although the theoretical framework of CMB lensing was established a decade ago, significant
observational progress has been made only recently. The lensing effect on CMB temperature and
polarization anisotropies as well as the gravitational lensing potential are now measured with both
ground-based and satellite experiments (e.g., [9–11], and see Sect. 5 for details), requiring studies of
more practical issues which are now rapidly developing. The measured lensing signals are already
used for some specific issues in cosmology, e.g., dark energy [12–15], dark matter [16], cosmic
strings [17], and primordial non-Gaussianity [18]. Although the statistical significance of the current

detections of lensing signals is not so high compared to other cosmological probes, the lensing signals obtained from upcoming and next-generation experiments will have enough potential to probe the following fundamental issues:

- *Dark energy, dark matter, and massive neutrinos:* The theoretical understanding of the nature of dark energy is still limited, and cosmological observations are the only way to reveal its dynamical properties. On the other hand, determination of the neutrino mass is one of the most important subjects in elementary particle physics, and is the key to understanding physics beyond the standard model of particle physics. The properties of dark energy, specific models of dark matter, and mass of neutrinos affect the evolution of gravitational potential, and thus the signals of weak lensing.
- *Gravitational waves, cosmic strings, and magnetic fields:* A measurement of the curl mode of deflection angles is also interesting for cosmology (see Sect. 2). The curl-mode deflection angles are produced by vector and tensor metric perturbations, but not by scalar perturbations. That is, the non-vanishing curl-mode signal is a smoking gun of non-scalar metric perturbations which can be sourced by gravitational waves [19–21] and cosmic strings [20,22,23] which may give clues about the mechanism of the inflationary scenario in the early universe and implications for high-energy physics. The magnetic fields at cosmological scales would also be probed with the curl mode. The rotation of the CMB polarization by the vector and tensor perturbations are also discussed in Ref. [24].

In addition, the study of CMB lensing has implications for detecting the signature of the primordial gravitational waves, since the amplitude of CMB B-mode polarization generated from primordial gravitational waves is smaller than that from lensing if the tensor-to-scalar ratio is very small [25]. In order to enhance sensitivity to the primordial B-mode polarization, subtraction of the lensed B-mode would become important [26–29]. Similarly, since the lensing induces non-Gaussian signatures in CMB anisotropies and non-zero off-diagonal elements in the covariance matrix, the lensing effect would be a possible confusing source in estimating the primordial non-Gaussianity or testing the statistical isotropy. For this reason, precise and accurate estimations of the lensing effect on CMB maps are required.

As the measurements of the lensing effect become more precise, the studies of CMB lensing should focus more on practical issues rather than on purely theoretical issues. For example, reconstruction of gravitational potential, which is mainly used for analysis of CMB lensing, is based on the assumption that the primordial CMB anisotropies are statistically isotropic. There are, however, several possible sources to generate mode couplings in the anisotropies such as the mask of Galactic emission and point sources [30,31], inhomogeneous noise [32], beam asymmetry [33], and so on. These contaminations potentially lead to a significant bias in the estimation of lensing potentials. For accurate cosmology with future observations, methods for mitigating all these biases are needed.

This paper is organized as follows. In Sect. 2, we formulate weak gravitational lensing in the presence of scalar, vector, and tensor metric perturbations, and see how the lensing signals depend on cosmological sources. In Sect. 3, we show how the lensing effect modifies the statistics of observed CMB anisotropies. In Sect. 4, we discuss the method for estimating the deflection angles and their power spectrum. Section 5 is devoted to a summary of the recent observational status and future prospects.

2. Weak gravitational lensing from scalar, vector, and tensor perturbations

Consider a photon emitted from the last scattering surface of the CMB, which passes through gravitational fields before reaching us. The geodesic of the photon is perturbed by the gravitational

lensing, and the photon is observed in a different direction from the original direction. The difference between observed and original directions is called the deflection angle, and provides information on the anisotropies of projected gravitational fields integrated from the last scattering surface to the observer. In this section, we review how the deflection angle is related to the gravitational fields and how its power spectrum depends on properties of several cosmological sources such as dark energy, massive neutrinos, and cosmic strings.

2.1.   Gradient and curl modes of deflection angle

The expression for the deflection angle with metric perturbations is obtained by solving the photon geodesic in a perturbed universe. Let us consider the line element given by

$$\mathrm{d}s^2 = a^2(\eta)(\bar{g}_{\mu\nu} + \delta g_{\mu\nu})\mathrm{d}x^\mu \mathrm{d}x^\nu, \tag{1}$$

where a is the scale factor in a homogeneous and isotropic universe, $\bar{g}_{\mu\nu}$ is the background unperturbed metric, and $\delta g_{\mu\nu}$ is the small metric perturbations. Here we assume that the unperturbed metric is described by the flat Friedman–Lemaître–Robertson–Walker metric:

$$\bar{g}_{\mu\nu}\mathrm{d}x^\mu \mathrm{d}x^\nu = -\mathrm{d}\eta^2 + \bar{\gamma}_{ij}\mathrm{d}x^i \mathrm{d}x^j = -\mathrm{d}\eta^2 + \mathrm{d}\chi^2 + \chi^2 \omega_{ab}\mathrm{d}\theta^a \mathrm{d}\theta^b, \tag{2}$$

with $\omega_{ab}\mathrm{d}\theta^a \mathrm{d}\theta^b = \mathrm{d}\theta^2 + \sin^2\theta \mathrm{d}\varphi^2$ denoting the metric on the unit sphere. In the conformal Newton gauge, the metric perturbations are described as[1]

$$\delta g_{00} = -2\Phi, \quad \delta g_{0i} = -\sigma_i, \quad \delta g_{ij} = 2\Psi\bar{\gamma}_{ij} + h_{ij}, \tag{3}$$

where the quantities Φ and Ψ are the scalar components, σ_i is the divergence-free vector component ($\sigma_i{}^{|i} = 0$), and h_{ij} is the transverse-traceless tensor component ($h_{ij}{}^{|i} = 0$, and $h^i{}_i = 0$). The vertical bar ($|$) denotes the covariant derivative with respect to the background three-dimensional metric, $\bar{\gamma}_{ij}$.

To define the deflection angle, let us consider null geodesics in the background and perturbed spacetime, $\bar{x}^\mu$ and x^μ. Since the photon path is not deflected in the background spacetime, the unperturbed path can be parametrized as $\bar{x}^\mu = (\eta_0 - \chi, \chi\hat{n}^i)$. Here the quantity η_0 denotes the conformal time today and $\hat{n}^i$ is the unit vector describing the observed direction of photon. Assuming a static observer, we define the deflection angle by projecting the angular components of the deviation vector $x^\mu - \bar{x}^\mu$ on the sphere [23]:

$$d^a \equiv \frac{[x^i(\chi_\mathrm{s}) - \bar{x}^i(\chi_\mathrm{s})]e_i{}^a}{\chi_\mathrm{s}} - \theta_O^a, \tag{4}$$

where the subscript a means the angular components θ and φ. The three-dimensional vectors $e_i{}^a$ are the basis vectors orthogonal to $\hat{n}^i$, the quantity χ_s is the conformal distance between the observer and the last scattering surface of the CMB, and θ_O^a is the angular coordinate at the observer. Since the deflection angle has two degrees of freedom, we decompose the deflection angle into two components by parity symmetry as [19,20,35,36]

$$d^a = \phi^{:a} + \epsilon^a{}_b \varpi^{:b}, \tag{5}$$

where (:) is the covariant derivative on the unit sphere, and $\epsilon^a{}_b$ denotes the two-dimensional Levi–Civita symbol. Hereafter, we call the first and second terms in the right-hand side of Eq. (5) the gradient and curl modes, respectively.

---

[1] Note that Ref. [23] gives the derivation of deflection angles in terms of the gauge-invariant variables in linear perturbation theory [34].

The deviation vector is obtained from the geodesic equation in the perturbed spacetime, and the resultant expressions for the gradient and curl modes are given by [23]

$$\nabla^2 \phi = d^a{}_{:a} = \int_0^{\chi_s} \frac{d\chi}{\chi} \left\{ \frac{\chi_s - \chi}{\chi_s} \nabla^2 [2\psi + \mathcal{A}] - \mathcal{B}^a{}_{:a} \right\},$$ (6)

$$\nabla^2 \varpi = d^a{}_{:b} \epsilon^b{}_a = -\int_0^{\chi_s} \frac{d\chi}{\chi} \mathcal{B}^a{}_{:b} \epsilon^b{}_a.$$ (7)

Here ∇^2 is the Laplacian operator on the unit sphere, $\psi = (\Phi - \Psi)/2$, and we define the quantities generated by non-scalar perturbations:

$$\mathcal{A} = \sigma_i \hat{n}^i + h_{ij} \hat{n}^i \hat{n}^j, \quad \mathcal{B}_a = \sigma_i e_a^i - 2h_{ij} e_a^i \hat{n}^j.$$ (8)

In Eqs. (6) and (7), the integral on the right-hand side is evaluated along the unperturbed light path, usually referred to as the Born approximation (see, e.g., Ref. [37] for the correction terms). The radial displacement (or the time delay) is also discussed in Ref. [38], but is a negligible effect on statistical observables.

Equation (7) shows that the curl mode of the deflection angle vanishes if we consider the scalar perturbations alone, but it is produced by the vector and/or tensor components. Also, beyond the linear perturbation, the curl mode is generated, e.g., by the second order of the density perturbations [36,39].

It is also worth noting the relation between the deflection angle and the elements of the Jacobi matrix which is defined as the mapping between a source and an image plane. The relation between the deflection angle and the Jacobi matrix is obtained by solving the geodesic deviation equation. Denoting the symmetric-traceless part of the Jacobi matrix divided by χ_s as γ_{ab} (shear components), the relation becomes [23,40]

$$\gamma_{ab} = d_{\langle a:b \rangle} + \frac{1}{2} [h_{\langle ab \rangle}]_0^{\chi_s},$$ (9)

where, for any quantity, $X_{\langle ab \rangle} = (X_{ab} + X_{ba} - X^c{}_c \omega_{ab})/2$. The last term arises in the presence of tensor perturbations as a difference of coordinate system perturbed by the metric at the observer and source positions [41].

2.2. Angular power spectrum of gradient and curl modes

Once we measure the deflection angle, one of the useful quantities in cosmology is the angular power spectrum of fluctuations, rather than the fluctuations themselves. Here we turn to discuss the angular power spectrum of the gradient and curl modes, based on Eqs. (6) and (7). To see how the observable depends on properties of the cosmological sources, we also show the relation between the angular power spectrum and the power spectrum of metric perturbations.

2.2.1. Scalar perturbations alone.

Let us first consider the case in the presence of scalar perturbations alone, since it helps our understanding of derivation in the presence of non-scalar perturbations.

The fluctuations of gravitational potential are decomposed into Fourier modes with the scalar-mode function $Q^{(0)}(\boldsymbol{x}, \boldsymbol{k}) = e^{-i\boldsymbol{k} \cdot \boldsymbol{x}}$ as

$$\psi(\boldsymbol{x}, \eta) = \int \frac{d^3 \boldsymbol{k}}{(2\pi)^3} \psi_{\boldsymbol{k}}(\eta) Q^{(0)}(\boldsymbol{x}, \boldsymbol{k}).$$ (10)

Substituting the above equation into Eq. (6), we obtain

$$\nabla^2 \phi = 2 \int_0^{\chi_s} d\chi \frac{\chi_s - \chi}{\chi_s \chi} \int \frac{d^3 k}{(2\pi)^3} \psi_k(\eta) \nabla^2 Q^{(0)}(\chi \hat{n}, k). \tag{11}$$

The angular power spectrum is defined as

$$\delta_{\ell\ell'} \delta_{mm'} C_\ell^{\phi\phi} = \langle \phi_{\ell m} \phi_{\ell'm'}^* \rangle, \tag{12}$$

where the quantities $\phi_{\ell m}$ are the spherical harmonic coefficients of the gradient mode and are defined with the spin-0 spherical harmonics $Y_{\ell m}(\hat{n})$ as

$$\phi(\hat{n}) = \sum_{\ell,m} \phi_{\ell m} Y_{\ell m}^*(\hat{n}). \tag{13}$$

Substituting the above equation into Eq. (11), and using the orthogonality of the spherical harmonics, we obtain[2]

$$\phi_{\ell m} = \frac{2}{\ell(\ell+1)} \int_0^{\chi_s} d\chi \frac{\chi_s - \chi}{\chi_s \chi} \int \frac{d^3 k}{(2\pi)^3} \psi_k(\eta) \int d^2\hat{n}\, Y_{\ell m}(\hat{n}) \nabla^2 Q^{(0)}(\chi \hat{n}, k), \tag{14}$$

where we use $\nabla^2 Y_{\ell,m} = \ell(\ell+1) Y_{\ell,m}$. To simplify the above equation, we use

$$\int d^2\hat{n}\, Y_{\ell m}(\hat{n}) \nabla^2 Q^{(0)}(\chi \hat{n}, k) = 4\pi(-i)^\ell j_\ell(k\chi)\ell(\ell+1) Y_{\ell m}^*(\hat{k}), \tag{15}$$

where $j_\ell(x)$ is the spherical Bessel function. Substituting the above equation into Eq. (14), we obtain

$$\phi_{\ell m} = 2 \int_0^{\chi_s} d\chi \frac{\chi_s - \chi}{\chi_s \chi} \int \frac{d^3 k}{2\pi^2} (-i)^\ell j_\ell(k\chi) \psi_k(\eta_0 - \chi) Y_{\ell m}^*(\hat{k}). \tag{16}$$

With the dimensionless power spectrum defined as

$$\langle \psi_k(\eta) \psi_{k'}^*(\eta') \rangle = (2\pi)^3 \delta(k - k') \frac{2\pi^2}{k^3} \Delta_\psi(k, \eta, \eta'), \tag{17}$$

the angular power spectrum of the gradient mode defined in Eq. (12) is given by

$$C_\ell^{\phi\phi} = 16\pi \int \frac{dk}{k} \int_0^{\chi_s} d\chi \int_0^{\chi_s} d\chi' \frac{\chi_s - \chi}{\chi_s \chi} \frac{\chi_s - \chi'}{\chi_s \chi'} j_\ell(k\chi) j_\ell(k\chi') \Delta_\psi(k, \eta_0 - \chi, \eta_0 - \chi'). \tag{18}$$

2.2.2. General case. Next we consider the case in the presence of all types of metric perturbations. Similar to Eq. (10), the vector and tensor metric perturbations are also decomposed into Fourier

---

[2] Note that we ignore $\ell = 0$ mode since this mode produces the mean value of the gradient mode and is not observable using a measurement of deflection angles.

modes with the mode functions of vector $Q_i^{(\pm 1)}(\boldsymbol{x}, \boldsymbol{k})$ and tensor $Q_{ij}^{(\pm 2)}(\boldsymbol{x}, \boldsymbol{k})$, respectively [42]:

$$\sigma_i(\boldsymbol{x}, \eta) = \int \frac{\mathrm{d}^3 \boldsymbol{k}}{(2\pi)^3} \sum_{s=\pm 1} \sigma_{\boldsymbol{k}}^{(s)}(\eta) Q_i^{(s)}(\boldsymbol{x}, \boldsymbol{k}), \tag{19}$$

$$h_{ij}(\boldsymbol{x}, \eta) = \int \frac{\mathrm{d}^3 \boldsymbol{k}}{(2\pi)^3} \sum_{s=\pm 2} h_{\boldsymbol{k}}^{(s)}(\eta) Q_{ij}^{(s)}(\boldsymbol{x}, \boldsymbol{k}), \tag{20}$$

where the explicit forms of these mode functions are given by [42]

$$Q_i^{(\pm 1)}(\boldsymbol{x}, \boldsymbol{k}) = \frac{\pm \mathrm{i}}{\sqrt{2}} e_{\pm, i}(\hat{\boldsymbol{k}}) \mathrm{e}^{-\mathrm{i}\boldsymbol{k}\cdot\boldsymbol{x}}, \tag{21}$$

$$Q_{ij}^{(\pm 2)}(\boldsymbol{x}, \boldsymbol{k}) = \frac{-1}{\sqrt{2}} e_{\pm, i}(\hat{\boldsymbol{k}}) e_{\pm, j}(\hat{\boldsymbol{k}}) \mathrm{e}^{-\mathrm{i}\boldsymbol{k}\cdot\boldsymbol{x}}. \tag{22}$$

Here the polarization vector $\boldsymbol{e}_\pm(\hat{\boldsymbol{k}}) = \boldsymbol{e}_\theta(\hat{\boldsymbol{k}}) \pm \mathrm{i}\boldsymbol{e}_\varphi(\hat{\boldsymbol{k}})$ is perpendicular to the wave vector $\boldsymbol{k}$. Similar to the case of the scalar perturbations alone, we first substitute Eqs. (19) and (20) into Eqs. (6) and (7). From Eq. (8), we then compute the similar form of Eq. (15) but for, e.g., $\nabla^2 \hat{n}^i Q_i^{(\pm 1)}$ instead of $\nabla^2 Q^{(0)}$. More generally, what we must compute is a quantity $\mathcal{J}_\ell^{(G)}(k\chi)$ defined as

$$\int \mathrm{d}^2 \hat{\boldsymbol{n}}\, Y_{\ell m}(\hat{\boldsymbol{n}}) G(\chi \hat{\boldsymbol{n}}, \boldsymbol{k}) = \mathcal{J}_\ell^{(G)}(k\chi) Y_{\ell m}^*(\hat{\boldsymbol{k}}), \tag{23}$$

where G is, for example, $\nabla^2 \hat{n}^i Q_i^{(\pm 1)}$. Reference [42] obtained the functional form of $\mathcal{J}^{(G)}$ (see also Refs. [23,43]) and applied it to the calculation of the CMB angular power spectrum. As shown in Ref. [23], Eq. (23) also simplifies the computation of the angular power spectra for the gradient and curl modes. To relate the angular power spectrum of the gradient and curl modes to the dimensionless power spectrum of the metric perturbations, we assume that the statistical properties of the vector and tensor modes are given by

$$\langle [\sigma_{\boldsymbol{k}}^{(s)}(\eta)]^* \sigma_{\boldsymbol{k}'}^{(s')}(\eta') \rangle = \delta_{ss'} \frac{1}{2} (2\pi)^3 \delta(\boldsymbol{k} - \boldsymbol{k}') \frac{2\pi^2}{k^3} \Delta^{(s)}(k; \eta, \eta') \qquad (s, s' = \pm 1), \tag{24}$$

$$\langle [h_{\boldsymbol{k}}^{(s)}(\eta)]^* h_{\boldsymbol{k}'}^{(s')}(\eta') \rangle = \delta_{ss'} \frac{1}{8} (2\pi)^3 \delta(\boldsymbol{k} - \boldsymbol{k}') \frac{2\pi^2}{k^3} \Delta^{(s)}(k; \eta, \eta') \qquad (s, s' = \pm 2). \tag{25}$$

The angular power spectrum of the curl mode $C_\ell^{\varpi\varpi}$ and the cross power spectrum between the gradient and curl modes $C_\ell^{\phi\varpi}$ are also defined in the same form as Eq. (12). The resultant angular power spectra are decomposed into the contributions from the scalar, vector, and tensor perturbations as [23]

$$C_\ell^{xx} = 4\pi \int_0^\infty \frac{\mathrm{d}k}{k} k^2 \int_0^{\chi_{\mathrm{s}}} \mathrm{d}\chi \int_0^{\chi_{\mathrm{s}}} \mathrm{d}\chi'$$
$$\times \sum_{s=-2}^{2} S_{x,\ell}^{(s)}(k\chi_{\mathrm{s}}, k\chi) S_{x,\ell}^{(s)}(k\chi_{\mathrm{s}}, k\chi') \Delta^{(s)}\left(k; \eta_0 - \chi, \eta_0 - \chi'\right), \tag{26}$$
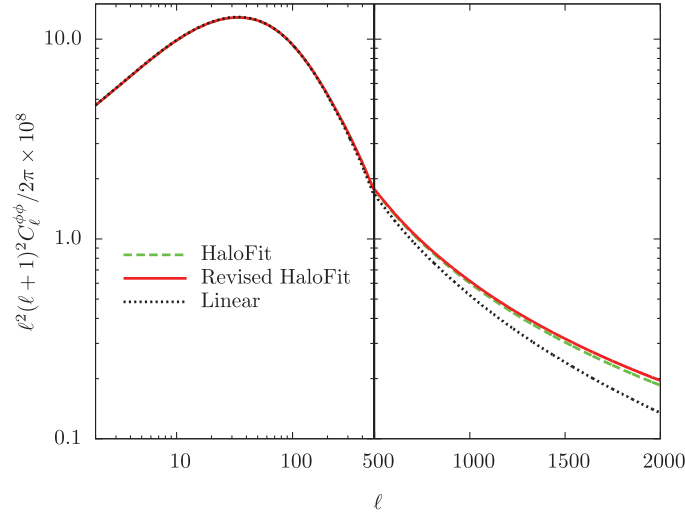
and $C_\ell^{\phi\varpi} = 0$, where $x = \phi$ or ϖ. The expressions of the transfer function, $S_{x,\ell}^{(s)}(\lambda, \lambda')$, are summarized as follows:

∘ scalar perturbations:

$$S_{\phi,\ell}^{(0)}(\lambda, \lambda') = 2 \frac{\lambda - \lambda'}{\lambda \lambda'} j_\ell(\lambda'), \tag{27}$$

$$S_{\varpi,\ell}^{(0)}(\lambda, \lambda') = 0. \tag{28}$$

Fig. 1. The angular power spectrum of the gradient mode generated by matter density fluctuations with the linear matter power spectrum (black dotted), and with the fitting formula of the non-linear matter power spectrum given in Refs. [44] (green dashed) or [45] (red solid).

○ vector perturbations:

$$S_{\phi,\ell}^{(\pm 1)}(\lambda, \lambda') = \sqrt{\frac{(\ell+1)!}{2(\ell-1)!}} \left[\frac{\lambda - \lambda'}{\lambda\lambda'} \frac{j_\ell(\lambda')}{\lambda'} - \frac{1}{\ell(\ell+1)} \frac{1}{(\lambda')^2} \frac{d[\lambda' j_\ell(\lambda')]}{d\lambda'} \right], \qquad (29)$$

$$S_{\varpi,\ell}^{(\pm 1)}(\lambda, \lambda') = \pm \sqrt{\frac{1}{2\ell(\ell+1)}} j_\ell(\lambda'), \qquad (30)$$

○ tensor perturbations:

$$S_{\phi,\ell}^{(\pm 2)}(\lambda, \lambda') = \sqrt{\frac{(\ell+2)!}{32(\ell-2)!}} \left[\frac{\lambda - \lambda'}{\lambda\lambda'} \frac{j_\ell(\lambda')}{\lambda'} - \frac{2}{\ell(\ell+1)} \frac{1}{(\lambda')^3} \frac{d[\lambda' j_\ell(\lambda')]}{d\lambda'} \right] + \frac{\delta_{\ell,2}}{10\sqrt{3}} \delta(\lambda'), \qquad (31)$$

$$S_{\varpi,\ell}^{(\pm 2)}(\lambda, \lambda') = \pm \sqrt{\frac{(\ell+2)!}{(\ell-2)!}} \frac{1}{2\ell(\ell+1)} \frac{j_\ell(\lambda')}{\lambda'}. \qquad (32)$$

2.2.3. Angular power spectrum of gradient and curl modes. Figure 1 shows the angular power spectrum of the gradient mode generated by the matter density fluctuations. Three lines show the cases with different fitting formulas of the matter power spectrum, i.e., the halofit model [44] and its revised formula [45], in calculating the angular power spectrum. For comparison, we also show the case with the linear power spectrum. Note that the lensing power spectrum is computed with CAMB [46]. The linear approximation to the matter power spectrum would be accurate at the scales where the signal becomes large ($\ell \sim 10$–100). The non-linear growth of matter density perturbations enhances the amplitude by 20–30% at $\ell \sim 2000$ compared to linear theory. The sensitivity of $C_\ell^{\phi\phi}$ to the models of the non-linear evolution would be not so significant even at these scales, because the lensing power spectrum computed with the halofit model of Ref. [44] is only a few percent smaller than the revised formula.
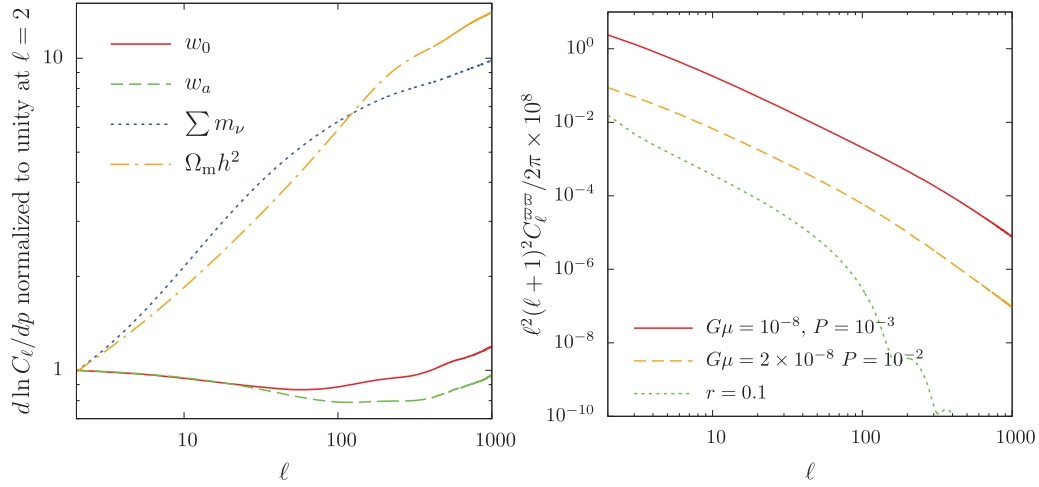
Fig. 2. *Left* : Logarithmic derivatives of the gradient-mode power spectrum $d \ln C_\ell^{\phi\phi}/dp$ with respect to the dark-energy equation-of-state parameters w_0 (red solid), w_a (green dashed), total mass of neutrinos $\sum m_\nu$ (blue dotted), and $\Omega_m h^2$ (orange long-dashed). The derivatives are normalized with the value at $\ell = 2$. Note that the sign of the derivative with respect to $\Omega_m h^2$ is positive, while the others have negative sign. *Right* : The angular power spectrum of the curl mode generated by primordial gravitational waves with tensor-to-scalar ratio $r = 0.1$ (green dotted) and a specific model of the cosmic string network (red solid/orange dashed).

In the left panel of Fig. 2, to see how the angular power spectrum depends on cosmological sources, we show the logarithmic derivatives of the angular power spectrum $C_\ell^{\phi\phi}$ with respect to w_0 and w_a, a parameterization of the dark-energy equation-of-state as $w = w_0 + (1 - a)w_a$, and the total mass of neutrinos $\sum m_\nu$. For comparison, we also show the dependence on the matter density $\Omega_m h^2$. Note that the derivatives are normalized with the value at $\ell = 2$. The derivatives with respect to the neutrino mass depend on ℓ, since the presence of the massive neutrinos suppresses the matter density fluctuations at smaller scales than their free-streaming scale after they become non-relativistic particles [47]. On the other hand, the derivatives with respect to w_0 and w_a are almost scale independent because the density fluctuations are affected by the properties of dark energy through the evolution of the scale factor in the linear perturbation regime. These behaviors imply that the power spectrum of the gradient mode can distinguish the effect of the neutrino mass from that of the dark energy through the scale dependence [48]. We note, however, that there exist some parameters that exhibit a similar scale dependence to the total neutrino mass, which can be a source of parameter degeneracy (see, e.g., [49]). As shown in Fig. 2, the logarithmic derivative with respect to the matter density gives a similar trend to that of the neutrino mass. This is because the matter density changes not only the amplitude of matter density fluctuations but also shifts the peak of the matter power spectrum which is determined by the radiation–matter equality. Within the CMB data set, the degeneracy between the total mass of neutrinos and matter density remains and other external datasets would be required to break this degeneracy.

On the other hand, in the right panel of Fig. 2 we show examples of the curl-mode angular power spectrum generated by primordial gravitational waves with tensor-to-scalar ratio $r = 0.1$, and a specific model of cosmic string networks [50] parametrized by the tension $G\mu$ and reconnection probability P. The angular power spectrum decreases at smaller scales since the perturbations are suppressed at sub-horizon scale. That is, a measurement of the curl-mode power spectrum on a large scale is important to probe the primordial gravitational waves and cosmic string networks.

3. Lensing effect on CMB anisotropies

The lensing effect on CMB anisotropies modifies the statistical properties of the observed CMB anisotropies. The non-Gaussian behavior in the lensed anisotropies is particularly important for measuring the angular power spectrum of the gradient and curl modes as discussed in the next section. In this section, we briefly summarize the weak lensing effect on the angular power spectrum of CMB temperature and polarization, and non-Gaussian statistics such as the bispectrum and trispectrum, in the presence of both the gradient and curl modes (see also Ref. [51] for a review of the effects on non-Gaussian statistics by lensing).

3.1.   Lensed CMB angular power spectrum

The lensed temperature anisotropies $\widetilde{\Theta}(\hat{\boldsymbol{n}})$ are expressed as a remapping of the unlensed temperature anisotropies $\Theta(\hat{\boldsymbol{n}})$ by a deflection angle (e.g., [1]):

$$\widetilde{\Theta}(\hat{\boldsymbol{n}}) = \Theta(\hat{\boldsymbol{n}} + \boldsymbol{d}(\hat{\boldsymbol{n}})). \tag{33}$$

The lensing effect on the CMB polarization is also described as a remapping of the Stokes parameters $Q \pm \mathrm{i}U$ by the deflection angle.

To analyze the asymptotic property of the lensed angular power spectrum, it is convenient to express the angular power spectrum in the flat-sky approximation. If we consider a small patch on a unit sphere and ignore the sky curvature, the CMB anisotropies are approximately given on a two-dimensional plane. In this limit, the lensed temperature anisotropies are expanded in terms of the plane wave:

$$\widetilde{\Theta}(\hat{\boldsymbol{n}}) = \int \frac{\mathrm{d}^2\boldsymbol{\ell}}{(2\pi)^2} \widetilde{\Theta}_{\boldsymbol{\ell}} \mathrm{e}^{\mathrm{i}\boldsymbol{\ell}\cdot\hat{\boldsymbol{n}}}. \tag{34}$$

On the other hand, since the lensed polarization anisotropies $\widetilde{Q} \pm \mathrm{i}\widetilde{U}$ are spin ± 2 quantities, we define the rotationally invariant quantities $\widetilde{E}_{\boldsymbol{\ell}}$ and $\widetilde{B}_{\boldsymbol{\ell}}$, usually referred to as E and B modes:

$$[\widetilde{Q} \pm \mathrm{i}\widetilde{U}](\hat{\boldsymbol{n}}) = -\int \frac{\mathrm{d}^2\boldsymbol{\ell}}{(2\pi)^2} (\widetilde{E}_{\boldsymbol{\ell}} \pm \mathrm{i}\widetilde{B}_{\boldsymbol{\ell}}) \mathrm{e}^{\pm\mathrm{i}2\varphi_{\boldsymbol{\ell}}} \mathrm{e}^{\mathrm{i}\boldsymbol{\ell}\cdot\hat{\boldsymbol{n}}}. \tag{35}$$

Here $\varphi_{\boldsymbol{\ell}}$ is the azimuthal angle measured from the x-axis of the two-dimensional plane. We can also expand the unlensed CMB anisotropies and define $\Theta_{\boldsymbol{\ell}}$, $E_{\boldsymbol{\ell}}$, and $B_{\boldsymbol{\ell}}$ in the same way. The lensed (unlensed) angular power spectrum $\widetilde{C}_{\ell}$ is then defined with the Fourier multipoles as

$$\langle \widetilde{X}_{\boldsymbol{\ell}} \widetilde{Y}_{\boldsymbol{\ell}'} \rangle = (2\pi)^2 \delta(\boldsymbol{\ell} - \boldsymbol{\ell}') \widetilde{C}_{\ell}^{XY} \qquad (X, Y = \Theta, E, B). \tag{36}$$

A method to obtain the angular power spectrum is to expand the lensed anisotropies in terms of the deflection angle up to the second order of the deflection angle [52]:

$$_{s}\widetilde{\Xi}(\hat{\boldsymbol{n}}) = {}_{s}\Xi(\hat{\boldsymbol{n}}) + d^a {}_{s}\Xi_{:a}(\hat{\boldsymbol{n}}) + \frac{d^a d^b}{2} {}_{s}\Xi_{:ab}(\hat{\boldsymbol{n}}), \tag{37}$$

where $s = 0$ or ± 2 and we define $_{0}\Xi = \Theta$ and $_{\pm 2}\Xi = Q \pm \mathrm{i}U$. The lensed CMB anisotropies in Fourier space become [19,52]

$$_{s}\widetilde{\Xi}_{\boldsymbol{\ell}} = {}_{s}\Xi_{\boldsymbol{\ell}} - \sum_{x=\phi,\varpi} \int \frac{\mathrm{d}^2\boldsymbol{L}}{(2\pi)^2} [(\boldsymbol{\ell} - \boldsymbol{L}) \odot_x \boldsymbol{L}] x_{\boldsymbol{\ell}-\boldsymbol{L}} {}_{s}\Xi_{\boldsymbol{L}} \mathrm{e}^{\mathrm{i}s\varphi_{L,\ell}}$$
$$+ \frac{1}{2} \sum_{x,y=\phi,\varpi} \int \frac{\mathrm{d}^2\boldsymbol{L}}{(2\pi)^2} \int \frac{\mathrm{d}^2\boldsymbol{L}'}{(2\pi)^2} [\boldsymbol{L}' \odot_x \boldsymbol{L}][(\boldsymbol{\ell} - \boldsymbol{L} - \boldsymbol{L}') \odot_y \boldsymbol{L}'] x_{\boldsymbol{L}'} y_{\boldsymbol{\ell}-\boldsymbol{L}-\boldsymbol{L}'} {}_{s}\Xi_{\boldsymbol{L}} \mathrm{e}^{\mathrm{i}s\varphi_{L,\ell}}, \tag{38}$$

where $\varphi_{L,\ell} = \varphi_L - \varphi_\ell$ and, for arbitrary two-dimensional vectors **a** and **b**, we define the products $\odot_\phi$ and $\odot_\varpi$ as

$$\boldsymbol{a} \odot_\phi \boldsymbol{b} \equiv a_\theta b_\theta + a_\varphi b_\varphi, \qquad \boldsymbol{a} \odot_\varpi \boldsymbol{b} \equiv a_\varphi b_\theta - a_\theta b_\varphi. \tag{39}$$

Using Eq. (38) and denoting the unlensed CMB angular power spectrum as C_ℓ, the lensed angular power spectrum for temperature and polarization in the flat-sky approximation becomes [19,52]

$$\widetilde{C}_\ell^{\Theta\Theta} = b_\ell C_\ell^{\Theta\Theta} + \sum_{x=\phi,\varpi} \int \frac{d^2\boldsymbol{L}}{(2\pi)^2} [\boldsymbol{L} \odot_x (\boldsymbol{\ell} - \boldsymbol{L})]^2 C_{|\boldsymbol{\ell}-\boldsymbol{L}|}^{xx} C_L^{\Theta\Theta}, \tag{40}$$

$$\widetilde{C}_\ell^{\Theta E} = b_\ell C_\ell^{\Theta E} + \sum_{x=\phi,\varpi} \int \frac{d^2\boldsymbol{L}}{(2\pi)^2} [\boldsymbol{L} \odot_x (\boldsymbol{\ell} - \boldsymbol{L})]^2 C_{|\boldsymbol{\ell}-\boldsymbol{L}|}^{xx} C_L^{\Theta E} \cos 2\varphi_{L,\ell}, \tag{41}$$

$$\widetilde{C}_\ell^{EE} = b_\ell C_\ell^{EE} + \sum_{x=\phi,\varpi} \int \frac{d^2\boldsymbol{L}}{(2\pi)^2} [\boldsymbol{L} \odot_x (\boldsymbol{\ell} - \boldsymbol{L})]^2 C_{|\boldsymbol{\ell}-\boldsymbol{L}|}^{xx}$$
$$\times \frac{1}{2}[(C_L^{EE} + C_L^{BB}) + (C_L^{EE} - C_L^{BB}) \cos 4\varphi_{L,\ell}], \tag{42}$$

$$\widetilde{C}_\ell^{BB} = b_\ell C_\ell^{BB} + \sum_{x=\phi,\varpi} \int \frac{d^2\boldsymbol{L}}{(2\pi)^2} [\boldsymbol{L} \odot_x (\boldsymbol{\ell} - \boldsymbol{L})]^2 C_{|\boldsymbol{\ell}-\boldsymbol{L}|}^{xx}$$
$$\times \frac{1}{2}[(C_L^{EE} + C_L^{BB}) - (C_L^{EE} - C_L^{BB}) \cos 4\varphi_{L,\ell}], \tag{43}$$

where we assume that correlation between the gradient and curl modes vanishes, and define

$$b_\ell = 1 - \ell^2 \sum_{x=\phi,\varpi} \int \frac{d\ln L}{4\pi} L^4 C_L^{xx} = 1 - \frac{\ell^2}{2} \langle |\boldsymbol{d}|^2 \rangle. \tag{44}$$

The lensing effect on the polarization has an interesting feature [8]; even in the absence of the primary B-mode polarization, $C_\ell^{BB} = 0$, the spatial pattern of the lensed polarization anisotropies could have an odd-parity mode. This is because a curl-free pattern is modified at each position and the resultant pattern is no longer a pure E-mode pattern. Note that a few arcminutes deflection, $\langle |\boldsymbol{d}|^2 \rangle \sim \mathcal{O}(10^{-7})$ [53], leads to $\ell^2 \langle |\boldsymbol{d}|^2 \rangle/2 \sim \mathcal{O}(1)$ if $\ell \sim 2500$. At these scales, the above expression is no longer valid because Eqs. (40)–(43) ignore the higher-order terms $\mathcal{O}(C_\ell^{xx})$, and the more accurate approach of Refs. [5,8] is required in which the angular power spectrum is computed using the correlation function, and the higher-order terms are included non-perturbatively with an exponential function [54].

In Fig. 3, we plot the lensed angular power spectrum of the temperature (left) and B-mode polarization (right), where the angular power spectrum is computed with CAMB [46]. The acoustic peaks in the temperature power spectrum are smeared by the lensing effect, and this can be understood as follows. The acoustic peaks are determined by typical sizes of hot and cold temperature spots in the sky. Lensing changes the size distribution of these spots (some get bigger and some get smaller), smearing the acoustic peaks. At small scales, the temperature power spectrum is dominated by lensing due to the transfer of large-scale power to small scales, where the primary temperature fluctuations are damped. The lensing also affects the E-mode power spectrum in a similar way to the temperature case.

The B-mode power spectrum generated by the lensing effect is, on the other hand, a scale-independent spectrum on large scales ($\ell \lesssim 100$) which roughly corresponds to 5–6 μK arcmin white
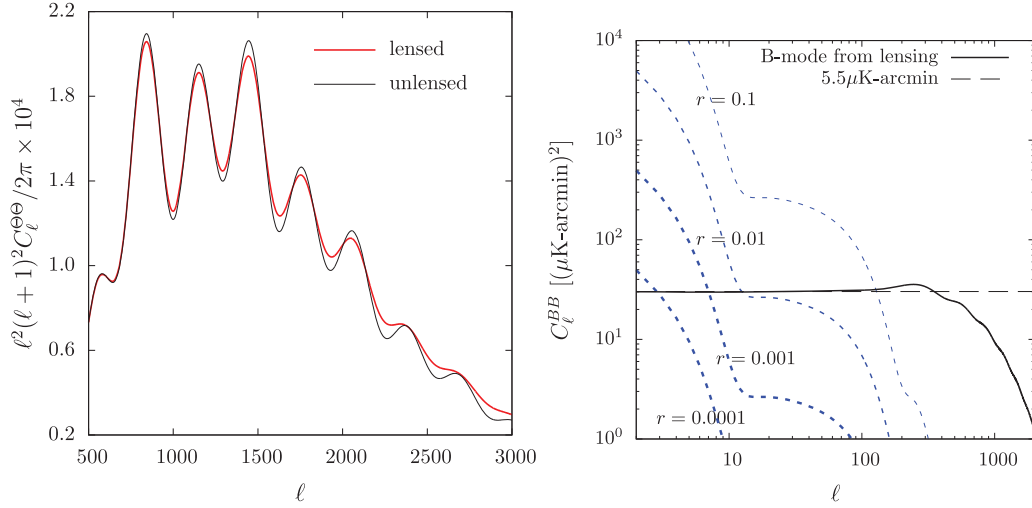
Fig. 3. Summary of important signatures in the angular power spectra of the lensed anisotropies compared to those of the unlensed anisotropies. Note that contributions from the curl mode $C_\ell^{\varpi\varpi}$ are ignored. *Left*: Comparison of the angular power spectra between the lensed (red) and unlensed (black) temperature anisotropies. For illustrative purposes, we multiply the angular power spectrum by $\ell^2(\ell+1)^2 \times 10^4/2\pi$. *Right*: The angular power spectrum of the B-mode polarization from the primordial gravitational waves (blue dotted), compared with that from the lensing (black solid). For the primordial gravitational waves, the tensor-to-scalar ratio r is varied from 0.1 to 0.0001. We also plot the white noise spectrum of 5.5 μK arcmin (black dashed).

noise. This would be considered as follows. The gradient of the primary E-mode has significant correlation on small scales, but does not correlate very much on scales larger than a few degrees (or $\ell \sim 100$ [28]). The lensing only remaps these small-scale fluctuations by typically a few arcminutes, and the resultant B-mode beyond degree scales is roughly an uncorrelated random field. This leads to the white noise spectrum on large scales.

As shown in Fig. 3, the primary B-mode power spectrum generated by the primordial gravitational waves is smaller than the lensing B-mode at the recombination bump ($\ell \sim 10$–100) if the tensor-to-scalar ratio is $r \lesssim 0.01$, and at the reionization bump ($\ell < 10$) if $r \lesssim 0.0001$ [25]. Therefore, if r is small, detection of the primary B-mode requires subtraction of the lensing B-mode, so called delensing (see, e.g., [28,55,56]).

3.2. Non-Gaussian signatures of lensed CMB anisotropies

3.2.1. Bispectrum. Assuming that the primary temperature anisotropies are a random Gaussian field, the three-point correlation $\langle \Theta_{\ell_1}\Theta_{\ell_2}\Theta_{\ell_3}\rangle$ vanishes. As described in Eq. (38), the lensing, however, induces mode couplings in the CMB anisotropies. The integrated Sachs–Wolfe (ISW)-lensing correlation then generates the three-point correlation of lensed CMB anisotropies as [57]

$$\langle \widetilde{\Theta}_{\boldsymbol{\ell}_1} \widetilde{\Theta}_{\boldsymbol{\ell}_2} \widetilde{\Theta}_{\boldsymbol{\ell}_3}\rangle = (2\pi)^2 \delta(\boldsymbol{\ell}_1 + \boldsymbol{\ell}_2 + \boldsymbol{\ell}_3)[C_{\ell_1}^{\Theta\phi} C_{\ell_2}^{\Theta\Theta} \boldsymbol{\ell}_1 \odot_\phi \boldsymbol{\ell}_2 + (\text{perms})] + \mathcal{O}(|d^a|^2). \qquad (45)$$

The ISW-lensing correlation generated by density perturbations on large scale, $C_\ell^{\Theta\phi}$, can be used to probe the late time evolution of the large-scale structure [7,57,58]. The cosmic strings at a late time of the universe also produce the temperature bispectrum through $C_\ell^{\Theta\phi}$ [59], but contributions from the curl mode vanish since the cross correlation of temperature and the curl mode is an odd-parity quantity. The curl mode generated by the cosmic strings would be, however, a source of the polarization bispectrum through, e.g., $C_\ell^{B\varpi}$. Note that the lensing bispectrum is a confusing source in estimating the primordial non-Gaussian signatures, especially for the squeezed type (e.g., $\ell_1 \sim \ell_2 \gg \ell_3$),

and the bias for the local type becomes $f_{\text{NL}} \sim \mathcal{O}(1)$ with ongoing and upcoming experiments [60–62]. The polarization bispectrum generated by lensing is also discussed in Ref. [63].

3.2.2. Trispectrum. The trispectrum of lensed CMB anisotropies has been explored [6,7,64] and can be used to estimate the power spectrum of the gradient and curl modes as discussed in the next section.

The four-point correlation of CMB anisotropies is in general decomposed into two terms as

$$\langle \widetilde{\Theta}_{\boldsymbol{\ell}_1} \widetilde{\Theta}_{\boldsymbol{\ell}_2} \widetilde{\Theta}_{\boldsymbol{\ell}_3} \widetilde{\Theta}_{\boldsymbol{\ell}_4} \rangle = \langle \widetilde{\Theta}_{\boldsymbol{\ell}_1} \widetilde{\Theta}_{\boldsymbol{\ell}_2} \widetilde{\Theta}_{\boldsymbol{\ell}_3} \widetilde{\Theta}_{\boldsymbol{\ell}_4} \rangle_{\text{d}} + \langle \widetilde{\Theta}_{\boldsymbol{\ell}_1} \widetilde{\Theta}_{\boldsymbol{\ell}_2} \widetilde{\Theta}_{\boldsymbol{\ell}_3} \widetilde{\Theta}_{\boldsymbol{\ell}_4} \rangle_{\text{c}}, \tag{46}$$

where the first term is the disconnected part expressed in terms of two point correlations as

$$\langle \widetilde{\Theta}_{\boldsymbol{\ell}_1} \widetilde{\Theta}_{\boldsymbol{\ell}_2} \widetilde{\Theta}_{\boldsymbol{\ell}_3} \widetilde{\Theta}_{\boldsymbol{\ell}_4} \rangle_{\text{d}} = \langle \widetilde{\Theta}_{\boldsymbol{\ell}_1} \widetilde{\Theta}_{\boldsymbol{\ell}_2} \rangle \langle \widetilde{\Theta}_{\boldsymbol{\ell}_3} \widetilde{\Theta}_{\boldsymbol{\ell}_4} \rangle + (\boldsymbol{\ell}_2 \leftrightarrow \boldsymbol{\ell}_3) + (\boldsymbol{\ell}_2 \leftrightarrow \boldsymbol{\ell}_4), \tag{47}$$

while the second term denotes the connected part which is not expressed in terms of the two point correlations of lensed anisotropies alone and reflects the non-Gaussian behavior of the fluctuations. The four-point correlation of the lensed temperature anisotropies has a contribution from the connected part as [65]

$$\langle \widetilde{\Theta}_{\boldsymbol{\ell}_1} \widetilde{\Theta}_{\boldsymbol{\ell}_2} \widetilde{\Theta}_{\boldsymbol{\ell}_3} \widetilde{\Theta}_{\boldsymbol{\ell}_4} \rangle_{\text{c}} \simeq (2\pi)^2 \delta(\boldsymbol{\ell}_1 + \boldsymbol{\ell}_2 + \boldsymbol{\ell}_3 + \boldsymbol{\ell}_4)$$
$$\times \sum_{x=\phi,\varpi} \left\{ C^{xx}_{|\boldsymbol{\ell}_1+\boldsymbol{\ell}_2|} f^x_{\boldsymbol{\ell}_1+\boldsymbol{\ell}_2,\boldsymbol{\ell}_1} f^x_{\boldsymbol{\ell}_3+\boldsymbol{\ell}_4,\boldsymbol{\ell}_3} + (\boldsymbol{\ell}_2 \leftrightarrow \boldsymbol{\ell}_3) + (\boldsymbol{\ell}_2 \leftrightarrow \boldsymbol{\ell}_4) \right\}, \tag{48}$$

where we define a weight function as

$$f^x_{\boldsymbol{L},\boldsymbol{L}'} = (\boldsymbol{L} \odot_x \boldsymbol{L}') C^{\Theta\Theta}_{L'} + (\boldsymbol{L}' \leftrightarrow \boldsymbol{L} - \boldsymbol{L}'). \tag{49}$$

In deriving Eq. (48), the lensed temperature anisotropies are expanded only up to the first order of the gradient and curl modes. The trispectrum of polarization generated by the lensing effect is also obtained analogously and the expression is given in Ref. [66].

3.2.3. Other statistics. There are also several papers discussing how the non-Gaussian signatures of the lensing effect change the statistical properties of a random Gaussian field, such as topological statistics [67,68], and the two-point correlation of hot spots [69,70]. Non-zero lensing trispectrum also modifies the covariance of the lensed CMB angular power spectrum [71–74].

4. Lensing reconstruction

Estimators for the lensing deflection fields in quadratic form of observed CMB anisotropies have been derived by several authors. References [75,76] developed a method for extracting lensing fields from temperature anisotropies with real space quantities. The method was subsequently extended to the case with polarization [77]. The quadratic estimator mostly used in the recent analysis was developed in Fourier space by Refs. [78,79] and [80] in flat and full sky, respectively, and was also extended to include the curl mode by Ref. [19] in flat sky and by Ref. [20] in full sky. On the other hand, the estimator is also derived in the context of the maximum likelihood [36,81]. These estimators all utilize the fact that a fixed gradient/curl mode introduces statistical anisotropy into the observed CMB, in the form of a correlation between the CMB anisotropies and its gradient. With a large number of observed CMB modes, this correlation may be used to form estimates of the gradient and curl modes. The lensing power spectrum, which is required for cosmological analysis, is then estimated from the gradient/curl mode estimators.

In this section, to see how to estimate the lensing power spectrum, $C_\ell^{\phi\phi}$ and $C_\ell^{\varpi\varpi}$, we first review the method for estimating the gradient and curl modes, usually referred to as lensing reconstruction, and their use of measuring the angular power spectrum (see also [82] for a detailed review on lensing reconstruction). Since the lensing fields will be measured more precisely in the near future, we also discuss the method for estimating lensing fields and their power spectrum with better accuracy.

4.1. Estimating CMB lensing potentials

4.1.1. Quadratic estimator for gradient and curl modes.
For simplicity, let us first consider an estimator with a CMB temperature map alone in the absence of curl modes. In the following, observed temperature anisotropies and their angular power spectrum are denoted as $\widehat{\Theta}_\ell$ and $\widehat{C}_\ell^{\Theta\Theta}$, respectively. We assume that the observed anisotropies are given by $\widehat{\Theta}_\ell = \widetilde{\Theta}_\ell + n_\ell$, where n_ℓ is the isotropic noise.

The observed direction of the lensed CMB at each position is shifted from the original direction according to the deflection angle, and the distance between two positions are modified at each position in a different way. For a fixed realization of the deflection angle, the correlation function of the primary CMB anisotropies depends not only on the distance between two positions but also on the position in the sky. In Fourier space, the lensing-induced anisotropy leads to correlations between two different Fourier modes of the observed CMB anisotropies:

$$\langle \widehat{\Theta}_L \widehat{\Theta}_{\ell-L} \rangle_{\mathrm{CMB,n}} = \phi_\ell f_{\ell,L}^\phi, \quad (\ell \neq 0) \tag{50}$$

where $f_{\ell,L}^\phi$ is given in Eq. (49), and we denote the ensemble average over primary CMB anisotropies and noise by $\langle \cdots \rangle_{\mathrm{CMB,n}}$, to distinguish it from the usual meaning of the ensemble average, $\langle \cdots \rangle$.

Based on Eq. (50), the quantity $\hat{\phi}_{\ell,L}$, defined as

$$f_{\ell,L}^\phi \hat{\phi}_{\ell,L} = \widehat{\Theta}_L \widehat{\Theta}_{\ell-L}, \tag{51}$$

is an estimator which satisfies the unbiased condition $\langle \hat{\phi}_{\ell,L} \rangle_{\mathrm{CMB,n}} = \phi_\ell$, where L is chosen so that $f_{\ell,L}^\phi \neq 0$. A more optimal and unbiased estimator can be obtained as a sum of $\hat{\phi}_{\ell,L}$ in terms of L, and the resultant estimator is [78]

$$\hat{\phi}_\ell = A_\ell^\phi \int \frac{\mathrm{d}^2 L}{(2\pi)^2} g_{\ell,L}^\phi \widehat{\Theta}_L \widehat{\Theta}_{\ell-L}. \tag{52}$$

Here the normalization, A_ℓ^ϕ, and the weight function, $g_{\ell,L}^\phi$, are given by

$$A_\ell^\phi = \frac{1}{[g^\phi, f^\phi]_\ell}; \quad g_{\ell,L}^\phi = \frac{f_{\ell,L}^\phi}{2\widehat{C}_L^{\Theta\Theta} \widehat{C}_{|\ell-L|}^{\Theta\Theta}}, \tag{53}$$

where, for convenience, the inner product is defined as

$$[g^x, f^y]_\ell \equiv \int \frac{\mathrm{d}^2 L}{(2\pi)^2} g_{\ell,L}^x f_{\ell,L}^y. \tag{54}$$

In the presence of the curl mode, Eq. (50) includes the additional term induced by the curl mode:

$$\langle \widehat{\Theta}_L \widehat{\Theta}_{\ell-L} \rangle_{\mathrm{CMB,n}} = \phi_\ell f_{\ell,L}^\phi + \varpi_\ell f_{\ell,L}^\varpi. \tag{55}$$

Even in this case, the estimator for the gradient mode is the same as in Eq. (52), at least, if we consider the first order of the gradient and curl modes. This is because the property of the parity symmetry is different for the gradient and curl modes, and the inner product $[f^\phi, f^\varpi]_\ell$, which leads

to a bias in the gradient-mode estimator, vanishes [20]. The quadratic estimators with the polarization anisotropies are also constructed in the same way as in the temperature case. The optimal quadratic estimator is finally obtained by combining all quadratic combinations of temperature and polarization fluctuations with the appropriate weight functions [79].

4.1.2. Practical cases. In practical situations, any non-lensing anisotropies arising from the masking [13,31,83], inhomogeneous map noise [32], and the beam asymmetry coupled with the scan strategy [33] will also generate the off-diagonal elements in the covariance matrix similar to Eq. (50), and the quadratic estimator is biased, i.e., $\langle \hat{x}_\ell \rangle_{\mathrm{CMB,n}} \neq 0$. In the case of polarization, there are also several possible sources generating mode couplings such as the temperature to polarization leakage, rotation of polarization basis, and so on [84].

To see this, let us consider a modulation on temperature anisotropies given by

$$\widehat{\Theta}(\hat{\boldsymbol{n}}) = (1 + \epsilon(\hat{\boldsymbol{n}}))(\widetilde{\Theta}(\hat{\boldsymbol{n}}) + n(\hat{\boldsymbol{n}})), \tag{56}$$

where $\epsilon(\hat{\boldsymbol{n}})$ may be regarded as the window function, inhomogeneity of the optical depth [85,86], Doppler boosting [87,88], and so on. The off-diagonal covariance of temperature anisotropies in the absence of the curl mode is given, at the first order, by

$$\langle \widehat{\Theta}_{\boldsymbol{L}} \widehat{\Theta}_{\boldsymbol{\ell}-\boldsymbol{L}} \rangle_{\mathrm{CMB,n}} = f^\phi_{\boldsymbol{\ell},\boldsymbol{L}} \phi_\ell + f^\epsilon_{\boldsymbol{\ell},\boldsymbol{L}} \epsilon_\ell, \tag{57}$$

where $f^\epsilon_{\boldsymbol{\ell},\boldsymbol{L}} = \widehat{C}^{\Theta\Theta}_L + \widehat{C}^{\Theta\Theta}_{|\boldsymbol{\ell}-\boldsymbol{L}|}$. Substituting the above equation into Eq. (52), we obtain

$$\langle \hat{\phi}_\ell \rangle_{\mathrm{CMB,n}} = \phi_\ell + R^{\phi,\epsilon}_\ell \epsilon_\ell, \tag{58}$$

where the response function, $R^{\phi,\epsilon}_\ell$, or in general, $R^{a,b}_\ell$, is defined as

$$R^{a,b}_\ell = \frac{A^{a,a}_\ell}{A^{a,b}_\ell}; \qquad A^{a,b}_\ell = \frac{1}{[g^a, f^b]_\ell}. \tag{59}$$

The second term of Eq. (58) is called the mean-field bias, and must be corrected.

One of the methods to correct the mean-field bias is to construct an estimator for ϵ_ℓ. Similar to the lensing estimator, the estimator for ϵ_ℓ is constructed using the weight function $f^\epsilon_{\boldsymbol{\ell},\boldsymbol{L}}$ instead of $f^\phi_{\boldsymbol{\ell},\boldsymbol{L}}$. The estimator of ϵ_ℓ is, however, biased by the presence of lensing as

$$\langle \hat{\epsilon}_\ell \rangle_{\mathrm{CMB,n}} = \epsilon_\ell + R^{\epsilon,\phi}_\ell \phi_\ell, \tag{60}$$

where $R^{\epsilon,\phi}_\ell$ is defined in Eq. (59). Combining Eqs. (58) and (60) to eliminate the term proportional to ϵ_ℓ, we find an unbiased estimator for the gradient mode:

$$\hat{\phi}'_\ell = \frac{\hat{\phi}_\ell - R^{\phi,\epsilon}_\ell \hat{\epsilon}_\ell}{1 - R^{\phi,\epsilon}_\ell R^{\epsilon,\phi}_\ell}. \tag{61}$$

Note that the above estimator is derived as the optimal estimator in the case when ϕ_ℓ and ϵ_ℓ are simultaneously estimated.

Even if we know the property of ϵ_ℓ (e.g., the window function), the estimator defined in Eq. (61) is useful as a cross check of systematics propagated from imperfect understanding of underlying CMB anisotropies [83]. A similar method can also be applied to reduce the inmohogeneous noise, unresolved point sources, polarization angle systematics [14,83], as well as for polarization-based reconstruction to reduce bias from the temperature-to-polarization leakage, rotation of polarization basis, and so on [89].

4.1.3. Maximum likelihood estimator.   Here we comment on the maximum likelihood estimator of Refs. [36,81] (see also Ref. [82] for a thorough review). Given a set of observed CMB anisotropies, we can formally derive the estimator for the lensing fields based on maximizing the likelihood. Although the numerical calculation of the maximum likelihood estimator is difficult compared to the quadratic estimator, it is possible to improve the precision of the estimated gradient and curl modes. For the gradient mode, the expression of the maximum likelihood estimator is nearly identical to that of the quadratic estimator if we only use the temperature anisotropies for the lensing reconstruction [81]. On the other hand, as shown in Ref. [36], the maximum likelihood estimator with the B-mode polarization significantly improves the sensitivity to the lensing signals, compared to the quadratic estimator. This is because the sensitivity of the maximum likelihood estimator is limited by the intrinsic scatter of the *primary* CMB anisotropies while the sensitivity of the quadratic estimator is limited by the *lensed* CMB anisotropies. These situations would be similar for the curl mode, also. The quadratic estimator is still useful for experiments with the polarization sensitivity of $\gtrsim 5\,\mu$K arcmin which corresponds to the amplitude of the B-mode polarization at $\ell \lesssim 1000$.

4.2. Estimating CMB lensing power spectrum

The angular power spectrum of the gradient and curl modes may be studied through the angular power spectrum of the estimators discussed in the previous section. The angular power spectrum of the quadratic estimators, however, includes additional contributions from, e.g., the four-point correlation of the lensed CMB anisotropies, and methods to accurately estimate these bias terms are required.

   To see this, from Eq. (52), we consider the angular power spectrum of the quadratic estimator with temperature which is given by

$$\langle |\widehat{x}_{\boldsymbol{\ell}}|^2 \rangle = (A_{\ell}^x)^2 \int \frac{\mathrm{d}^2 \boldsymbol{L}}{(2\pi)^2} \int \frac{\mathrm{d}^2 \boldsymbol{L}'}{(2\pi)^2} \frac{f_{\ell,L}^x}{2\widehat{C}_L^{\Theta\Theta}\widehat{C}_{|\boldsymbol{\ell}-\boldsymbol{L}|}^{\Theta\Theta}} \frac{f_{\ell,L'}^x}{2\widehat{C}_{L'}^{\Theta\Theta}\widehat{C}_{|\boldsymbol{\ell}-\boldsymbol{L}'|}^{\Theta\Theta}} \langle \widehat{\Theta}_{\boldsymbol{L}}\widehat{\Theta}_{\boldsymbol{\ell}-\boldsymbol{L}}(\widehat{\Theta}_{\boldsymbol{L}'}\widehat{\Theta}_{\boldsymbol{\ell}-\boldsymbol{L}'})^* \rangle. \quad (62)$$

This quantity probes the four-point function of the lensed CMB. Following Eq. (46), we decompose the above quantity into disconnected and connected parts:

$$\langle |\hat{x}_{\boldsymbol{\ell}}|^2 \rangle = \langle |\hat{x}_{\boldsymbol{\ell}}|^2 \rangle_{\mathrm{d}} + \langle |\hat{x}_{\boldsymbol{\ell}}|^2 \rangle_{\mathrm{c}}. \quad (63)$$

The disconnected part, $\langle \cdots \rangle_{\mathrm{d}}$, which comes from Eq. (47), contains the contributions which would be expected if the observed temperature anisotropies $\widehat{\Theta}_{\boldsymbol{L}}$ were a Gaussian random variable. On the other hand, the connected part, $\langle \cdots \rangle_{\mathrm{c}}$, arising from Eq. (48) has the non-Gaussian contributions which are a distinctive signature of lensing. As shown in the following, the connected part nearly corresponds to the power spectrum of the gradient/curl mode, and therefore the disconnected part, usually referred to as "Gaussian bias," and the other bias terms must be accurately subtracted to obtain a clean measurement of the lensing signals.

   Let us discuss the explicit expression of the disconnected and connected part.

○ *Disconnected part*:
   Using Eq. (47), the explicit form of the Gaussian bias is written as

$$\langle \widehat{\Theta}_{\boldsymbol{L}}\widehat{\Theta}_{\boldsymbol{\ell}-\boldsymbol{L}}(\widehat{\Theta}_{\boldsymbol{L}'}\widehat{\Theta}_{\boldsymbol{\ell}-\boldsymbol{L}'})^* \rangle_{\mathrm{d}} = (2\pi)^2 [\delta_D(\boldsymbol{L}+\boldsymbol{L}') + \delta_D(\boldsymbol{L}+\boldsymbol{L}'-\boldsymbol{\ell})]\widehat{C}_L^{\Theta\Theta}\widehat{C}_{|\boldsymbol{\ell}-\boldsymbol{L}|}^{\Theta\Theta}. \quad (64)$$

Substituting Eq. (64) into Eq. (62), and using the expression for the normalization A_{ℓ}^x, the power spectrum of the estimator induced by the disconnected part becomes

$$N_{\ell}^{x,(0)} \equiv \langle |\widehat{x}_{\boldsymbol{\ell}}|^2 \rangle_{\mathrm{d}} = \left\{ \int \frac{\mathrm{d}^2 \boldsymbol{L}}{(2\pi)^2} \frac{(f_{\ell,L}^x)^2}{2\widehat{C}_L^{\Theta\Theta}\widehat{C}_{|\boldsymbol{\ell}-\boldsymbol{L}|}^{\Theta\Theta}} \right\}^{-1} = A_{\ell}^x. \quad (65)$$

○ *Connected part*:

Substituting Eq. (48) into Eq. (62), the connected part of the quadratic estimator is, on the other hand, given by [65]

$$\langle |\hat{x}_{\boldsymbol{\ell}}|^2 \rangle_{\mathrm{c}} = C_\ell^{xx} + N_\ell^{x,(1)} + \mathcal{O}[(C_\ell^{xx})^2]. \tag{66}$$

Here C_ℓ^{xx} is the gradient-mode power spectrum which we wish to estimate, while $N_\ell^{x,(1)}$ is a nuisance term coming from the "secondary" lensing contractions of the trispectrum [64] which is usually called the N1 bias.

Combining Eqs. (65) and (66) with Eq. (63), we obtain

$$\langle |\hat{x}_{\boldsymbol{\ell}}|^2 \rangle = C_\ell^{xx} + N_\ell^{x,(0)} + N_\ell^{x,(1)} + \mathcal{O}[(C_\ell^{xx})^2]. \tag{67}$$

The above equation means that the lensing power spectrum C_ℓ^{xx} is measured by computing the power spectrum of the lensing estimator and subtracting the accurate estimation of bias terms such as $N_\ell^{x,(0)}$ and $N_\ell^{x,(1)}$.

The Gaussian bias is usually larger than the gradient/curl-mode power spectrum for reconstructions with a noisy map. A method to improve sensitivity to C_ℓ^{xx} is to use an observed map filtered by a realization-dependent power spectrum instead of its ensemble-averaged quantities [90] in Eq. (65). In addition, the realization-dependent estimate has an advantage in reducing the off-diagonal covariance, $\langle \widehat{C}_\ell^{\phi\phi} \widehat{C}_{\ell'}^{\phi\phi} \rangle$ [91]. For practical situations in which the covariance of the observed map has non-negligible off-diagonal components, the following estimator is useful as a realization-dependent approach [83]:

$$\widehat{N}_\ell^{x,(0)} = (A_\ell^x)^2 \frac{1}{2} \int \frac{\mathrm{d}^2 \boldsymbol{L}}{(2\pi)^2} \int \frac{\mathrm{d}^2 \boldsymbol{L}'}{(2\pi)^2} f_{\boldsymbol{\ell},\boldsymbol{L}}^x f_{\boldsymbol{\ell},\boldsymbol{L}'}^x \left(2\overline{\boldsymbol{C}}_{\boldsymbol{L},\boldsymbol{\ell}-\boldsymbol{L}'} \overline{\Theta}_{\boldsymbol{\ell}-\boldsymbol{L}} \overline{\Theta}_{\boldsymbol{L}'}^* - \overline{\boldsymbol{C}}_{\boldsymbol{L},\boldsymbol{\ell}-\boldsymbol{L}'} \overline{\boldsymbol{C}}_{\boldsymbol{\ell}-\boldsymbol{L},\boldsymbol{L}'} \right). \tag{68}$$

Here, $\overline{\Theta}_{\boldsymbol{\ell}} \equiv \sum_{\boldsymbol{\ell}'} \boldsymbol{C}_{\boldsymbol{\ell},\boldsymbol{\ell}'}^{-1} \widehat{\Theta}_{\boldsymbol{\ell}'}$ is the inverse-variance filtered multipoles and $\overline{\boldsymbol{C}}_{\boldsymbol{\ell},\boldsymbol{\ell}'}$ is the covariance of $\overline{\Theta}$. The above estimator is naturally derived based on the optimal estimator of the trispectrum [92] applied to lensing [14,83], and is easily extended to include polarization [89]. Equation (68) has an additional advantage for accurate estimation of C_ℓ^{xx}; if the covariance is biased as $\overline{\boldsymbol{C}}_{\boldsymbol{\ell},\boldsymbol{\ell}'} \rightarrow \overline{\boldsymbol{C}}_{\boldsymbol{\ell},\boldsymbol{\ell}'} + \Sigma_{\boldsymbol{\ell},\boldsymbol{\ell}'}$, the contributions of $\Sigma_{\boldsymbol{\ell},\boldsymbol{\ell}'}$ in Eq. (68) are at second order, while the usual method has the first-order contributions of $\Sigma_{\boldsymbol{\ell},\boldsymbol{\ell}'}$. Another way to mitigate uncertainties in $N_\ell^{x,(0)}$ is that, since a large fraction of the noise in the lensing reconstruction comes from the CMB fluctuations themselves, we can construct a Gaussian-bias-free estimator by dividing the CMB multipoles into disjoint regions in Fourier space, with a cost of signal-to-noise [64,93]. For polarization-based reconstructions, the Gaussian bias is more simply mitigated by combining, e.g., EE and EB estimators since the four-point correlation $\langle EEEB \rangle_{\mathrm{d}}$ vanishes.

Other bias terms such as the N1 bias $N_\ell^{x,(1)}$ should be also corrected. Even in the absence of the curl mode, $N_\ell^{\varpi,(1)}$ is generated by the presence of the gradient mode [13,31]. Furthermore, Ref. [91] pointed out that the term including the second order of $C_\ell^{\phi\phi}$ in Eq. (67) also leads to non-negligible bias. This type of bias can be mitigated by replacing the *unlensed* power spectrum in the weight function with the *lensed* power spectrum [63,94]. The diagonal approximation of the normalization A_ℓ would also lead to a bias in estimating the power spectrum in the presence of, e.g., the window function. The bias due to this diagonal approximation in the presence of the masking and survey boundary is not so significant for the temperature-based reconstruction [83], but would be significant on large scales for polarization-based reconstruction. For known sources such as the window effect, we would estimate the normalization bias by Monte Carlo simulations, but cross checking with other

methods would be desirable as a test of the assumptions in the simulations, e.g., underlying CMB anisotropies.

Since the power spectrum of the quadratic estimator probes the four-point correlation of observed anisotropies, other possible sources of the four-point correlation may lead to significant bias on $\widehat{C}_{\ell'}^{xx}$. One of the significant trispectrum sources is the point sources [14], and Ref. [95] constructed an estimator for mitigating the point-source trispectrum by modeling the statistical properties of the point sources, while Ref. [96] proposed a simulation-based approach. The bias on estimates of the power spectrum due to the presence of primordial non-Gaussianity would also be a source of the trispectrum but is negligible even even if $f_{\mathrm{NL}} \sim \mathcal{O}(10)$ [97].

In estimating cosmological parameters with the gradient/curl-mode power spectrum, the angular power spectrum of observed CMB maps is usually added to break degeneracies between parameters. One concern in this case is the correlation of the angular power spectrum between lensed CMB and deflection angles. Assuming a Planck-like experiment with temperature alone, this correlation is negligible [98]. The covariance of the angular power spectrum of lensing fields is investigated in Refs. [65,91], and is almost diagonal for this case.

5. Recent experimental progress and future prospects

5.1. Current status of observations

Observations of the lensing effect on CMB are rapidly improving (see Table 1). Combining the Arcminute Cosmology Bolometer Array Receiver (ACBAR) with the Wilkinson Microwave Anisotropy Probe (WMAP) data, Ref. [9] reported weak evidence of the lensing effect on the temperature power spectrum by constraining a parameter q which characterizes the lensing effect as $C_{\ell}^{\mathrm{lens}} = C_{\ell}^{\mathrm{no-lens}} + q(C_{\ell}^{\mathrm{lens}} - C_{\ell}^{\mathrm{no-lens}})$. On the other hand, Ref. [116] showed a constraint on the lensing amplitude A by replacing $C_{\ell}^{\phi\phi} \to A C_{\ell}^{\phi\phi}$ in computing the lensed temperature power spectrum, and found $A = 3.0_{-0.9}^{+0.9}$, while Ref. [9] showed $A = 1.60_{-0.26}^{+0.55}$. The lensing effect on the temperature power spectrum has also been explored by several high-resolution experiments such as the Atacama Cosmology Telescope (ACT) [117] and South Pole Telescope (SPT) [118,119]. The recent Planck result [15] showed clear evidence for the lensing effect on the temperature power spectrum at $\gtrsim 10\,\sigma$ statistical significance.[3] The polarization signals have also been used to show evidence for the lensing effect on the CMB anisotropies. The recent SPTpol results showed the detection of B-mode polarization signals generated from the lensing effect by cross-correlating a map of the cosmic-infrared background obtained from Herschel [11]. Using the polarization data obtained from the PolarBear experiment, the B-mode maps were also used to measure the B-mode angular power spectrum [120].

As shown in Fig. 4, the power spectrum of the gradient mode obtained through the lensed CMB trispectrum has also been explored by several CMB experiments. The power spectrum has been measured at $\sim 4\,\sigma$–$6\,\sigma$ significance based on the ACT [10,99] or SPT [13] temperature maps. At the time of writing this paper, the most precise measurement of the power spectrum is given by Planck with greater than $25\,\sigma$ detection [14]. CMB polarization maps from the SPTpol [11] and PolarBear [111] are also utilized to measure the gradient-mode power spectrum. As shown in Fig. 5, the curl-mode power spectrum has been measured with ACT [17], SPT [13], and Planck temperature maps [14], and is consistent with zero.

---

[3] Note that $A > 1$ is favored at $\sim 2\,\sigma$ [15].

Table 1. Current observational status of the measurement of the CMB lensing power spectrum and cross power spectrum with other data. Each column shows the gradient-mode power spectrum ($\phi \times \phi$), the cross correlation with the galaxy/quasar catalog ($\phi \times G$), the cosmic infrared background map ($\phi \times$CIB) or other probes such as the cosmic shear ($\phi \times \gamma$), the integrated Sachs–Wolfe effect ($\phi \times$ISW), and thermal Sunyaev–Zel'dovich effect ($\phi \times$tSZ). Note that part of the results is obtained by combining additional data e.g., WMAP. We also note that the lensing effect has been measured from the power spectrum of CMB anisotropies with several experiments (see text for details).

	Temperature			
	$\phi \times \phi$	$\phi \times$G	$\phi \times$CIB	$\phi \times$ other probes
ACT	$4\,\sigma$ [10] $4.6\,\sigma$ [99]	$3.8\,\sigma$ [100]	—	$3.2\,\sigma$ [101] ($\times\gamma$)
Planck	$26\,\sigma$ [14]	$7\,\sigma$–$20\,\sigma$ [14]	$42\,\sigma$ [102][a]	$2.5\,\sigma$ [103] ($\times$ISW) $6.2\,\sigma$ [104] ($\times$tSZ)
SPT	$6.3\,\sigma$ [13]	4.2–$5.3\,\sigma$ [105] $\sim 7\,\sigma$ [107]	$8.8\,\sigma$ [106]	— —
WMAP	—[b]	$\sim 3\,\sigma$ [108–110][c]	—	—[d]
	Polarization			
	$\phi \times \phi$	$\phi \times$G	$\phi \times$CIB	$\phi \times$ other probes
PolarBear	$\sim 2\,\sigma$ [111][e]	—	$4.0\,\sigma$ [112]	—
SPTpol	$\sim 3\,\sigma$ [11][f]	—	$7.7\,\sigma$ [11]	—

[a] Statistical significance at 545 GHz.

[b] Ref. [113] showed that the significance is $\lesssim 1$–$2\,\sigma$.

[c] The measurement of the cross correlation was first attempted by Ref. [114], but the signals were not detected.

[d] Statistical significance of cross correlation with the sum of SZ and ISW is at $\lesssim 1$–$2\,\sigma$ [115].

[e] The statistical significance for the rejection of the null hypothesis is at $4.6\,\sigma$.

[f] Ref. [11] constrained the lensing amplitude as a consistency test.
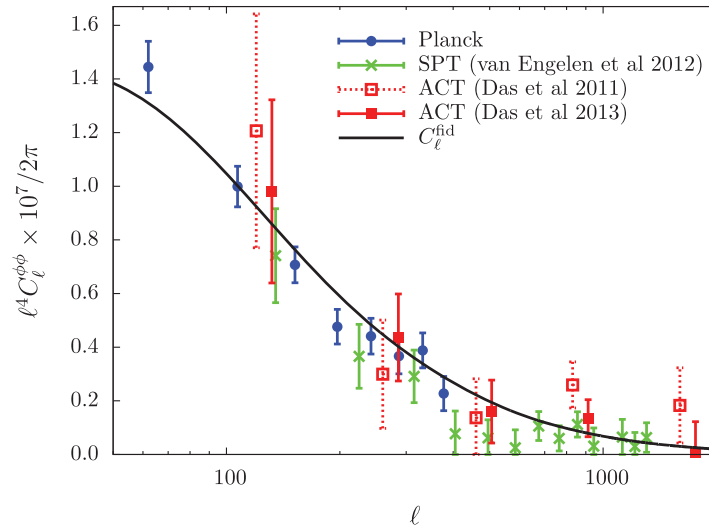
Fig. 4. Measurements of the angular power spectrum of the gradient mode obtained from Planck [14], SPT [13], and ACT [10,99], with temperature-based lensing reconstruction. The solid line shows the theoretical power spectrum expected from the best-fit cosmological parameters to the Planck temperature data.
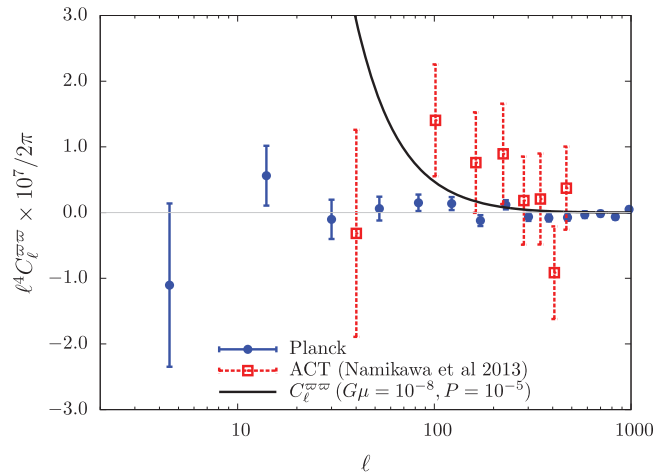
Fig. 5. As Fig. [4] but for the curl mode obtained from Planck [14] and ACT temperature map [17]. The solid line shows the theoretical power spectrum for a specific model of cosmic string network with $G\mu = 10^{-8}$ and $P = 10^{-5}$. Note that the curl mode from SPT temperature data is also analyzed in Ref. [13].

There are also several efforts to measure the cross correlation between the CMB lensing and other observables. Cross correlation with matter density fluctuations is detected at 2–3 σ significance with the data set of WMAP and observations of the large-scale structure such as the Sloan Digital Sky Survey (SDSS) and the NRAO VLA Sky Survey (NVSS) [108,109]. The first detection of the cross correlation was made earlier than the measurements of the gradient-mode power spectrum. The galaxy/quasar–CMB lensing cross correlation has also been measured by Refs. [14,100,105]. Cross correlations with maps of the cosmic infrared background have also been measured and utilized to estimate the bias factor of dusty sources [106] and the star formation rate [102]. This correlation is more significant than the cross correlation with the galaxy/quasar number density since the cosmic infrared background is sensitive to the density fluctuations of dark matter mostly around $z \sim 2$, corresponding to the peak of the CMB lensing kernel [121]. Reference [101] reported a measurement of the cross correlation with the cosmic shear using data from ACT and the Canada–France–Hawaii Telescope (CFHT) Stripe 82 Survey (CS82). Measurements of cross correlations with other CMB secondaries such as the integrated Sachs–Wolfe effect and thermal Sunyaev–Zel'dovich effect are reported in Refs. [103] and [104], respectively.

Lensing signals are now one of the standard probes in cosmology, and have already been used for several cosmological issues. The inclusion of the gradient-mode power spectrum breaks degeneracies of parameters involved in the angular-diameter distance to the last scattering [122], e.g., the dark energy density Ω_Λ and curvature parameter Ω_K, whose degeneracies are difficult to break with the primary CMB anisotropies alone [123–125] (see also [126] concerning the numerical effect which breaks degeneracies). As shown in Refs. [12–14], combining the lensing signals with the primary CMB anisotropies provides the evidence for dark energy with CMB data alone, and the constraints on the dark energy density without any astrophysical data is now $\Omega_\Lambda = 0.67^{+0.027}_{-0.023}$ (1 σ) [14]. There have been several studies which used cross correlation for some specific issues. Using cross correlation between the lensing and galaxy survey, constraints on the primordial non-Gaussianity parameter through a measurement of the galaxy bias are obtained as $f_{NL} = 12 \pm 21$ (1 σ) [18]. Reference [127] used the Planck lensing map to constrain the bias of the Wide-Field Infrared Survey Explorer (WISE) for the purpose of estimating the ISW effect. As discussed in Sect. [2], the curl mode of lensing signals

also has fruitful information on the non-scalar perturbations. Figure 5 shows the measured curl-mode power spectrum compared with that produced by the cosmic string network. The measured curl-mode power spectrum is used for excluding the parameter region of cosmic strings [17] which is not ruled out by the current data of the temperature power spectrum [50,128].

5.2.   *Future prospects*

CMB polarization data on an arcminute scale will soon become the best way to obtain the CMB lensing power spectrum and cross correlations, and these precise signals will play an important role in cosmology in the near future (see, e.g., Ref. [129] and references therein). This will be achieved by ongoing ground-based experiments such as ACTPol,[4] PolarBear,[5] and SPTpol,[6] and upcoming/next-generation experiments, e.g., Polar,[7] CMBPol,[8] COrE,[9] and PRISM.[10]

Based on the above planned experiments, let us discuss the future prospects in CMB lensing studies. For the neutrinos, assuming upcoming/next-generation experiments and combining the gradient-mode power spectrum with the primary CMB power spectrum, 1σ constraints on the total mass of neutrinos would be 35–60 meV (e.g., [48,49,130,131]). On the other hand, the 1σ constraint on the effective number of neutrinos will be $\sim$0.1 [130].

The cross-correlation studies with CMB lensing will also become important in the future. Inclusion of cross correlations with other observables will further improve the constraints on the total mass of the neutrinos (e.g., [132,133] and references therein). For example, if we combine the Stage-II class experiments with other ongoing projects such as the Subaru Hyper Suprime-Cam,[11] the constraints on neutrino mass would be 40 meV [49]. In the future, with the Stage-IV class experiments and other upcoming spectroscopic surveys, the constraints on the mass of neutrinos and effective number of neutrinos would be $\sim$16 meV and 0.02, respectively [133]. This implies that the lower bound on the neutrino mass $\sum m_\nu \sim 60$ meV obtained from neutrino oscillation experiments would be detected at 4σ confidence level with future experiments.

For upcoming and future experiments, the auto and cross power spectrum between CMB lensing and other observables would have sensitivity to probe the dark-energy equation-of-state parameters (e.g., [49,122,134]), a specific model of dark energy (e.g., [131,134])/modified gravity (e.g., [116]), the primordial non-Gaussianity through measurement of galaxy bias (e.g., [135]), and the cosmic string network (e.g., [22]). In addition to probing the above advanced issues, cross correlation with other probes will help to control systematics such as multiplicative bias and intrinsic alignment in the cosmic shear analysis (e.g., [136–139]).

In the future, as mentioned in Sect. 3, delensing may be required to obtain the primary B-mode signals at the recombination bump ($\ell \sim 10$–100). The B-mode signal at these scales would be important for ground-based experiments in which the large-scale modes are difficult to obtain. The delensing at the recombination bump is also important for future low-resolution space missions such as

---

[4] http://www.princeton.edu/act/
[5] http://bolo.berkeley.edu/polarbear/
[6] http://pole.uchicago.edu/
[7] http://polar-array.stanford.edu/
[8] http://cmbpol.uchicago.edu/
[9] http://www.core-mission.org/
[10] http://www.prism-mission.org/
[11] http://www.naoj.org/Projects/HSC/index.html

LiteBIRD[12] and PIXIE [140] in order to enhance the total signal-to-noise of the primary B-mode as well as the sensitivity to the tensor spectral index which allows us to explore the details of inflationary physics. Joint analysis for, e.g., LiteBIRD and ground-based CMB experiments would reveal the primordial B-mode signals from the largest scale to the recombination bump, providing us with much information on the primordial gravitational waves. The above estimates and prospects are, however, discussed in simple and idealistic situations, and studies aiming at addressing practical issues are much needed as data become precise.

Acknowledgements

References

[1] A. Blanchard and J. Schneider, Astron. Astrophys., **184**, 1 (1987).
[2] M. Sasaki, Mon. Not. Roy. Astron. Soc., **240**, 415 (1989).
[3] K. Tomita and K. Watanabe, PTEP, **82**, 563 (1989).
[4] T. Fukushige, J. Makino, and T. Ebisuzaki, Astrophys. J., **436**, L107 (1994).
[5] U. Seljak, Astrophys. J., **463**, 1 (1996).
[6] F. Bernardeau, Astron. Astrophys., **324**, 15 (1997).
[7] M. Zaldarriaga, Phys. Rev. D, **62**, 063510 (2000).
[8] M. Zaldarriaga and U. Seljak, Phys. Rev. D, **58**, 023003 (1998).
[9] C. L. Reichardt et al., Astrophys. J., **694**, 1200 (2009).
[10] S. Das et al., Phys. Rev. Lett., **107**, 021301 (2011).
[11] D. Hanson et al., Phys. Rev. Lett., **111**, 141301 (2013).
[12] B. D. Sherwin et al., Phys. Rev. Lett., **107**, 021302 (2011).
[13] A. van Engelen et al., Astrophys. J., **756**, 142 (2012).
[14] Planck Collaboration, arXiv:1303.5077.
[15] Planck Collaboration, arXiv:1303.5076.
[16] R. J. Wilkinson, J. Lesgourgues, and C. Boehm, arXiv:1309.7588.
[17] T. Namikawa, D. Yamauchi, and A. Taruya, Phys. Rev. D **88**, 083525 (2013).
[18] T. Giannantonio and W. J. Percival, arXiv:1312.5154.
[19] A. Cooray, M. Kamionkowski, and R. R. Caldwell, Phys. Rev. D, **71**, 123527 (2005).
[20] T. Namikawa, D. Yamauchi, and A. Taruya, JCAP, **1201**, 007 (2012).
[21] H. Padmanabhan, A. Rotti, and T. Souradeep, Phys. Rev. D **88**, 063507 (2013).
[22] D. Yamauchi, T. Namikawa, and A. Taruya, JCAP, **1210**, 030 (2012).
[23] D. Yamauchi, T. Namikawa, and A. Taruya, JCAP, **1308**, 051 (2013).
[24] L. Dai, Phys. Rev. Lett., **112**, 041303 (2014).
[25] L. Knox and Y.-S. Song, Phys. Rev. Lett., **89**, 011303 (2002).
[26] L. Verde, H. Peiris, and R. Jimenez, JCAP, **0601**, 019 (2006).
[27] K. M. Smith et al., AIP Conf. Proc., **1141**, 121 (2009).
[28] K. M. Smith et al., JCAP, **1206**, 014 (2012).
[29] K. N. Abazajian et al., arXiv:1309.5381.
[30] C. S. Carvalho and K. Moodley, Phys. Rev. D, **81**, 123010 (2010).
[31] A. Benoit-Levy et al., Astron. Astrophys., **555**, 10 (2013).
[32] D. Hanson, G. Rocha, and K. Gorski, Mon. Not. Roy. Astron. Soc., **400**, 2169 (2009).
[33] D. Hanson, A. Lewis, and A. Challinor, Phys. Rev. D, **81**, 103003 (2010).

---

[12] http://cmbpol.kek.jp/litebird/index.html

[34] H. Kodama and M. Sasaki, PTEP Supp., **78**, 1 (1984).
[35] A. Stebbins, arXiv:astro-ph/9609149.
[36] C. M. Hirata and U. Seljak, Phys. Rev. D, **68**, 083002 (2003).
[37] A. Cooray and W. Hu, Astrophys. J., **574**, 19 (2002).
[38] W. Hu and A. Cooray, Phys. Rev. D, **63**, 023504 (2001).
[39] D. Sarkar et al., Phys. Rev. D, **77**, 103515 (2008).
[40] F. Schmidt and D. Jeong, Phys. Rev. D, **86**, 083513 (2012).
[41] S. Dodelson, E. Rozo, and A. Stebbins, Phys. Rev. Lett., **91**, 021301 (2003).
[42] W. Hu and M. J. White, Phys. Rev. D, **56**, 596 (1997).
[43] L. Dai, M. Kamionkowski, and D. Jeong, Phys. Rev. D, **86**, 125013 (2012).
[44] R. E. Smith et al., Mon. Not. Roy. Astron. Soc., **341**, 1311 (2003).
[45] R. Takahashi et al., Astrophys. J., **761**, 152 (2012).
[46] A. Lewis, A. Challinor, and A. Lasenby, Astrophys. J., **538**, 473 (2000).
[47] J. R. Bond, G. Efstathiou, and J. Silk, Phys. Rev. Lett., **45**, 1980 (1980).
[48] M. Kaplinghat, L. Knox, and Y.-S. Song, Phys. Rev. Lett., **91**, 241301 (2003).
[49] T. Namikawa, S. Saito, and A. Taruya, JCAP, **1012**, 027 (2010).
[50] D. Yamauchi et al., Phys. Rev. D, **85**, 103515 (2012).
[51] K. M. Smith, ASP Conf. Ser., **432**, 147 (2009).
[52] W. Hu, Phys. Rev. D, **62**, 043007 (2000).
[53] A. Lewis and A. Challinor, Phys. Rep., **429**, 1 (2006).
[54] A. Challinor and A. Lewis, Phys. Rev. D, **71**, 103010 (2005).
[55] U. Seljak and C. M. Hirata, Phys. Rev. D, **69**, 043005 (2004).
[56] W.-H. Teng, C.-L. Kuo, and J.-H. P. Wu, arXiv:1102.5729.
[57] D. M. Goldberg and D. N. Spergel, Phys. Rev. D, **59**, 103002 (1999).
[58] U. Seljak and M. Zaldarriaga, Phys. Rev. D, **60**, 043504 (1999).
[59] D. Yamauchi, Y. Sendouda, and K. Takahashi, arXiv:1309.5528.
[60] P. Serra and A. Cooray, Phys. Rev. D, **77**, 107305 (2008).
[61] A. Cooray, D. Sarkar, and P. Serra, Phys. Rev. D, **77**, 123006 (2008).
[62] D. Hanson et al., Phys. Rev. D, **80**, 083004 (2009).
[63] A. Lewis, A. Challinor, and D. Hanson, JCAP, **1103**, 018 (2011).
[64] W. Hu, Phys. Rev. D, **64**, 083005 (2001).
[65] M. H. Kesden, A. Cooray, and M. Kamionkowski, Phys. Rev. D, **67**, 123507 (2003).
[66] T. Okamoto and W. Hu, Phys. Rev. D, **66**, 063008 (2002).
[67] J. Schmalzing, M. Takada, and T. Futamase, Astrophys. J., **544**, L83 (2000).
[68] M. Takada, Astrophys. J., **558**, 29 (2001).
[69] M. Takada, E. Komatsu, and T. Futamase, Astrophys. J., **533**, L83 (2000).
[70] M. Takada and T. Futamase, Astrophys. J., **546**, 620 (2001).
[71] S. Smith, A. Challinor, and G. Rocha, Phys. Rev. D, **73**, 023517 (2006).
[72] K. M. Smith, W. Hu, and M. Kaplinghat, Phys. Rev. D, **74**, 123002 (2006).
[73] C. Li, T. L. Smith, and A. Cooray, Phys. Rev. D, **75**, 083501 (2007).
[74] A. Benoit-Levy, K. M. Smith, and W. Hu, Phys. Rev., **D86**, 123008 (2012).
[75] M. Zaldarriaga and U. Seljak, Phys. Rev. D, **59**, 123507 (1999).
[76] U. Seljak and M. Zaldarriaga, Phys. Rev. Lett., **82**, 2636 (1999).
[77] J. Guzik, U. Seljak, and M. Zaldarriaga, Phys. Rev. D, **62**, 043517 (2000).
[78] W. Hu, Astrophys. J., **557**, L79 (2001).
[79] W. Hu and T. Okamoto, Astrophys. J., **574**, 566 (2002).
[80] T. Okamoto and W. Hu, Phys. Rev. D, **67**, 083002 (2003).
[81] C. M. Hirata and U. Seljak, Phys. Rev. D, **67**, 043001 (2003).
[82] D. Hanson, A. Challinor, and A. Lewis, Gen. Rel. Grav., **42**, 2197 (2010).
[83] T. Namikawa, D. Hanson, and R. Takahashi, Mon. Not. Roy. Astron. Soc., **431**, 609 (2013).
[84] M. Shimon et al., Phys. Rev. D, **77**, 083003 (2008).
[85] V. Gluscevic, M. Kamionkowski, and D. Hanson, arXiv:1210.5507.
[86] J. O'Bryan et al., arXiv:1306.1232.
[87] Planck Collaboration, arXiv:1303.5087.
[88] D. Hanson and A. Lewis, Phys. Rev. D, **80**, 063004 (2009).
[89] T. Namikawa and R. Takahashi, Mon. Not. Roy. Astron. Soc., **438**, 1507 (2014).

[90] C. Dvorkin, W. Hu, and K. M. Smith, Phys. Rev. D, **79**, 107302 (2009).
[91] D. Hanson et al., Phys. Rev. D, **83**, 043005 (2011).
[92] D. M. Regan, E. P. S. Shellard, and J. R. Fergusson, Phys. Rev. D, **82**, 023520 (2010).
[93] B. D. Sherwin and S. Das, arXiv:1011.4510.
[94] E. Anderes, Phys. Rev. D, **88**, 083517 (2013).
[95] S. J. Osborne, D. Hanson, and O. Dore, arXiv:1310.7547.
[96] A. van Engelen et al., arXiv:1310.7023.
[97] J. Lesgourgues et al., Phys. Rev. D, **71**, 103514 (2005).
[98] M. M. Schmittfull et al., Phys. Rev. D, **88**, 063012 (2013).
[99] S. Das et al., arXiv:1301.1037.
[100] B. D. Sherwin et al., Phys. Rev. D, **86**, 083006 (2012).
[101] N. Hand et al., arXiv:1311.6200.
[102] Planck Collaboration, arXiv:1303.5078.
[103] Planck Collaboration, arXiv:1303.5079.
[104] J. C. Hill and D. N. Spergel, arXiv:1312.4525.
[105] L. E. Bleem et al., Astrophys. J., **753**, L9 (2012).
[106] G. P. Holder et al., Astrophys. J., **771**, L16 (2013).
[107] J.E. Geach et al., AJ, **776**, L41 (2013).
[108] K. M. Smith, O. Zahn, and O. Dore, Phys. Rev. D, **76**, 043510 (2007).
[109] C. M. Hirata et al., Phys. Rev. D, **78**, 043520 (2008).
[110] C. Feng et al., Phys. Rev. D, **86**, 063519 (2012).
[111] PolarBear Collaboration, arXiv:1312.6646.
[112] PolarBear Collaboration, arXiv:1312.6645.
[113] C. Feng et al., Phys. Rev. D, **85**, 043513 (2012).
[114] C. M. Hirata et al., Phys. Rev. D, **70**, 103501 (2004).
[115] E. Calabrese et al., Phys. Rev. D, **81**, 043529 (2010).
[116] E. Calabrese et al., Phys. Rev. D, **80**, 103516 (2009).
[117] S. Das et al., Astrophys. J., **729**, 62 (2011).
[118] R. Keisler et al., Astrophys. J., **743**, 28 (2011).
[119] K. T. Story et al., Astrophys. J., **779**, 86 (2013).
[120] PolarBear Collaboration, arXiv:1403.2369.
[121] Y.-S. Song et al., Astrophys.J., **590**, 664 (2003).
[122] W. Hu, Phys. Rev. D, **65**, 023003 (2002).
[123] M. Zaldarriaga, D. N. Spergel, and U. Seljak, Astrophys. J., **488**, 1 (1997).
[124] J. R. Bond, G. Efstathiou, and M. Tegmark, Mon. Not. Roy. Astron. Soc., **291**, L33 (1997).
[125] G. Efstathiou and J. R. Bond, Mon. Not. Roy. Astron. Soc., **304**, 75 (1999).
[126] C. Howlett et al., JCAP, **1204**, 027 (2012).
[127] S. Ferraro, B. D. Sherwin, and D. N. Spergel, arXiv:1401.1193.
[128] Planck Collaboration, arXiv:1303.5085.
[129] W. L. K. Wu et al., arXiv:1402.4108.
[130] J. Lesgourgues et al., Phys. Rev. D, **73**, 045021 (2006).
[131] R. de Putter, O. Zahn, and E. V. Linder, Phys. Rev. D, **79**, 065033 (2009).
[132] K. N. Abazajian et al., Astropart. Phys., **35**, 177 (2011).
[133] K. N. Abazajian et al., arXiv:1309.5383.
[134] S. Das and D. N. Spergel, Phys. Rev. D, **79**, 043509 (2009).
[135] Y. Takeuchi, K. Ichiki, and T. Matsubara, Phys. Rev. D, **85**, 043518 (2012).
[136] A. Vallinotto, Astrophys. J., **759**, 32 (2012).
[137] S. Das, J. Errard, and D. Spergel, arXiv:1311.2338.
[138] A. Hall and A. Taylor, arXiv:1401.6018.
[139] M. A. Troxel and M. Ishak, arXiv:1401.7051.
[140] A. Kogut et al., JCAP, **1107**, 025 (2011).